Mon. Not. R. Astron. Soc. **000**, 000–000 (0000) Printed 9 January 2012 (MN LATEX style file v2.2)

Broken discs: warp propagation in accretion discs

Christopher J. Nixon[1] and Andrew R. King[1]

[1] *Department of Physics & Astronomy, University of Leicester, Leicester LE1 7RH UK*

9 January 2012

ABSTRACT

We simulate the viscous evolution of an accretion disc around a spinning black hole. In general any such disc is misaligned, and warped by the Lense–Thirring effect. Unlike previous studies we use effective viscosities constrained to be consistent with the internal fluid dynamics of the disc. We find that nonlinear fluid effects, which reduce the effective viscosities in warped regions, can promote the breaking of the disc into two distinct planes. This occurs when the Shakura & Sunyaev dimensionless viscosity parameter α is $\lesssim 0.3$ and the initial angle of misalignment between the disc and hole is $\gtrsim 45^\circ$. The break can be a long–lived feature, propagating outwards in the disc on the usual alignment timescale, after which the disc is fully co– or counter–aligned with the hole. Such a break in the disc may be significant in systems where we know the inclination of the outer accretion disc to the line of sight, such as some X–ray binaries: the inner disc, and so any jets, may be noticeably misaligned with respect to the orbital plane.

Key words: accretion, accretion discs – black hole physics – galaxies: active – galaxies: evolution – galaxies: jets

1 INTRODUCTION

In realistic astrophysical situations the angular momentum of a spinning black hole may be significantly misaligned with respect to a surrounding accretion disc. This is expected in black hole X–ray binaries where the hole may have received a significant kick during formation (Shklovskii 1970; Sutantyo 1978; Arzoumanian, Chernoff & Cordes 2002; Hobbs et al. 2005). It is also likely for accretion on to a supermassive black hole (SMBH) in the centre of a galaxy. The scale of the SMBH is so small compared with the galaxy that any process which drives gas down to the galactic centre is unlikely to have any special orientation with respect to the SMBH spin. The spin direction is set by the SMBH's accretion history and not by whatever causes the next accretion event. Processes such as star formation, merging of satellite galaxies, gas cloud collisions and other galactic phenomena likely to drive gas inwards are chaotic, so it is reasonable to expect a random spread of angles between the angular momentum of infalling gas and that of the hole (cf King & Pringle 2006King & Pringle 2007; King, Pringle & Hofmann 2008). This gas is likely to form a ring around the SMBH which then viscously spreads into a misaligned accretion disc.

The Lense–Thirring (hereafter LT) effect of a spinning black hole causes non–equatorial orbits to precess at rates dependent on the distance from the hole (Lense & Thirring, 1918). In an accretion disc, this differential precession causes a warp which propagates through the disc. This is the Bardeen–Petterson effect (Bardeen & Petterson, 1975). In this paper we restrict our attention to viscous Keplerian accretion discs with negligible self–gravity. Papaloizou & Pringle (1983) linearised the equations of fluid dynamics to derive the first consistent equation governing the evolution of a warped disc of this type, assuming a tilt angle smaller than the disc angular semi–thickness. They introduced two effective kinematic viscosities controlling the angular momentum transport in the disc. In principle these two quantities depend on the nature of the warp: ν_1 governs the usual radial communication of the component of angular momentum perpendicular to the plane of the disc due to differential rotation (for a flat disc this is the Shakura & Sunyaev alpha viscosity), while ν_2 governs the radial communication of the component of angular momentum parallel to the local orbital plane; this acts to flatten tilted rings of gas. Papaloizou & Pringle (1983) also showed that conservation laws require a relation between ν_1 and ν_2. For small warps this is

$$\nu_2 = \frac{\nu_1}{2\alpha^2}, \tag{1}$$

where α is the usual dimensionless viscosity parameter for discs (Shakura & Sunyaev, 1973) assumed $\ll 1$ by Papaloizou & Pringle (1983). This gives

$$\alpha_2 = \frac{1}{2\alpha}, \tag{2}$$

(again for small α) where α_2 is an equivalent dimensionless viscosity parameter for ν_2.

Pringle (1992) derived an evolution equation valid for larger warps expressing global angular momentum conservation for a disc composed of rings of gas with no internal degrees of freedom.

⋆ E–mail: chris.nixon@astro.le.ac.uk

Pringle (1992) went on to develop a numerical technique for integrating this equation over rings of gas to study the viscous evolution of a time–dependent warped disc. Lodato & Pringle (2006) used this to study the Bardeen–Petterson effect. They assumed constant effective viscosities, related as expected for small amplitude warps (eq. 1). This treatment suggests that a disc warp must always straighten itself out on a timescale shorter than the accretion timescale (assuming only the LT torque and the internal disc torques, i.e. no other external torques), because (1) implies $\nu_2 \gg \nu_1$ for typical values of α. The realignment process enhances the accretion rate by inducing extra dissipation (Lodato & Pringle, 2006).

The analysis of Pringle (1992) did not allow for any internal degrees of freedom within the gas rings, and was described as the 'naive approach' in Papaloizou & Pringle (1983). However Ogilvie (1999) derived equations of motion directly from the full three–dimensional fluid dynamical equations with an assumed isotropic viscosity. This confirmed that the equations of Pringle (1992) are formally valid only when two differences are taken into account (or can be safely neglected). The first is that the Pringle (1992) equations omit a torque causing rings to precess if they are tilted with respect to their neighbours. In a viscous Keplerian disc where $\alpha \ll 1$ but not close to zero, this torque is much smaller than the usual viscous torques included by Pringle (1992) and so can be neglected in time–dependent calculations. (however for completeness we include the torque in this work). Our main focus, however, is on the second extension. The quantities ν_1 and ν_2 are functions of the disc structure and so depend on the warp amplitude $|\psi| = R\,|\partial \boldsymbol{\ell}/\partial R|$, where $\boldsymbol{\ell}$ is the unit angular momentum vector and R is the spherical radius coordinate. Ogilvie (1999) used the equations of fluid dynamics to determine the relation between the effective viscosities for a general warp amplitude. In contrast to an assumption of constant effective viscosities, this analysis suggests that these quantities *drop* in a warped region, making it much harder for the disc to straighten any twisted rings of gas. Indeed, if the warp becomes large enough the disc may break into distinct planes with only a tenuous connection. We expect this to occur in large warps, as nonlinear corrections to the fluid flow are significant for warp amplitudes $|\psi| \gtrsim \alpha$ (Ogilvie, 1999).

There have been several theoretical investigations which show evidence of breaking discs. Larwood & Papaloizou (1997) report an example in Smoothed Particle Hydrodynamics (SPH) simulations of a circumbinary disc with a strong radial density decrease. This is suggestive, since the evolution of a misaligned circumbinary disc is qualitatively similar to that of a misaligned disc around a spinning black hole (Nixon, King & Pringle, 2011). SPH simulations by Lodato & Price (2010) also found disc breaking. They assumed the presence of a large–amplitude warp and followed its viscous development. Their results agreed with those expected for the constrained viscosities derived in Ogilvie (1999), and showed that the disc could break if the warp amplitude was large enough (note that this paper did not attempt to show that the LT precession could *produce* such a warp).

In this paper we explore disc evolution under the LT effect with general warp amplitudes, and the effective viscosities constrained as in Ogilvie (1999). We explore the evolution for a range of α values and different degrees of misalignment between the disc and hole. We aim to discover if the internal torques in an accretion disc can sustain a smooth warped configuration under the LT torque, or whether instead the disc breaks into distinct planes.

2 NUMERICAL METHOD

2.1 Evolution equation

The problem of disc breaking is complex, and to make progress we adopt the simplest approach. We use a 1D Eulerian ring code of the type described in Pringle (1992) and used in Lodato & Pringle (2006). Our code has been adapted to include the third effective viscosity and the nonlinear fluid dynamical constraints found by Ogilvie (1999). Here '1D' means that the properties assigned to each ring depend only on its radius. Section 2.1 of Lodato & Pringle (2006) gives a detailed discussion of the validity of this approach. The main restriction is that the evolution of a disc warp must be diffusive rather than wave–like. Papaloizou & Pringle (1983) show that this holds if $\alpha > H/R$, which is usually satisfied for accretion discs around compact objects.

Our 1D ring code describes the evolution of warped accretion discs by evolving the angular momentum density vector of each ring $\boldsymbol{L}(R,t)$ through the equation

$$\begin{aligned}\frac{\partial \boldsymbol{L}}{\partial t} &= \frac{1}{R}\frac{\partial}{\partial R}\left\{\frac{(\partial/\partial R)\left[\nu_1 \Sigma R^3\left(-\Omega'\right)\right]}{\Sigma\,(\partial/\partial R)\,(R^2\Omega)}\boldsymbol{L}\right\} \\ &+ \frac{1}{R}\frac{\partial}{\partial R}\left[\frac{1}{2}\nu_2 R\,|\boldsymbol{L}|\,\frac{\partial \boldsymbol{\ell}}{\partial R}\right] \\ &+ \frac{1}{R}\frac{\partial}{\partial R}\left\{\left[\frac{\frac{1}{2}\nu_2 R^3\Omega\,|\partial\boldsymbol{\ell}/\partial R|^2}{(\partial/\partial R)\,(R^2\Omega)} + \nu_1\left(\frac{R\Omega'}{\Omega}\right)\right]\boldsymbol{L}\right\} \\ &+ \frac{1}{R}\frac{\partial}{\partial R}\left(\nu_3 R\,|\boldsymbol{L}|\,\boldsymbol{\ell}\times\frac{\partial \boldsymbol{\ell}}{\partial R}\right) \\ &+ \boldsymbol{\Omega}_{\rm p}\times\boldsymbol{L}\end{aligned} \tag{3}$$

where ν_1, ν_2 and ν_3 are the effective viscosities, $\Omega\,(R)$ is the local azimuthal angular velocity, $\Sigma\,(R)$ is the disc surface density, $\boldsymbol{\ell}\,(R)$ is the unit angular momentum vector, and $\boldsymbol{\Omega}_{\rm p}\,(R)$ is the precession frequency induced in the disc by the LT effect (defined below). We note that $\boldsymbol{L} = \Sigma R^2\Omega\boldsymbol{\ell}$.

Equation (3) shows that there are five independent torques acting on the rings of gas. The first four terms on the rhs represent the internal disc torques responsible for communicating angular momentum. The last term represents the LT torque. Here we briefly discuss these terms.

The first term on the rhs of (3) describes the usual viscous diffusion of mass. This is governed by the azimuthal shear viscosity ν_1. The second term is also diffusive. This term, governed by the vertical viscosity ν_2, is responsible for diffusing the disc tilt. The third term is an advective torque. Depending on its sign this advects angular momentum (and hence mass) inwards or outwards through the disc.

The three terms discussed above are exactly those derived straightforwardly from the conservation of mass and angular momentum (Pringle, 1992). The fourth term is a precessional torque found by the analysis in Ogilvie (1999). This torque causes rings to precess about $\boldsymbol{\ell}\times\frac{\partial\boldsymbol{\ell}}{\partial R}$ and thus only acts when the disc is tilted. This leads to a dispersive wave–like propagation of the warp (Ogilvie, 1999). The direction of the precession is dependent on α and $|\psi|$ (cf. Figure 5 in Ogilvie, 1999). This term has exactly the same form as the second term in (3) with the substitutions $0.5\nu_2 \rightarrow \nu_3$ and $\partial\boldsymbol{\ell}/\partial R \rightarrow \boldsymbol{\ell}\times\partial\boldsymbol{\ell}/\partial R$. This transformation shows that we can integrate this term using the technique described in Pringle (1992) for integrating the second term.

The fifth term is the LT torque arising from the gravitomag-

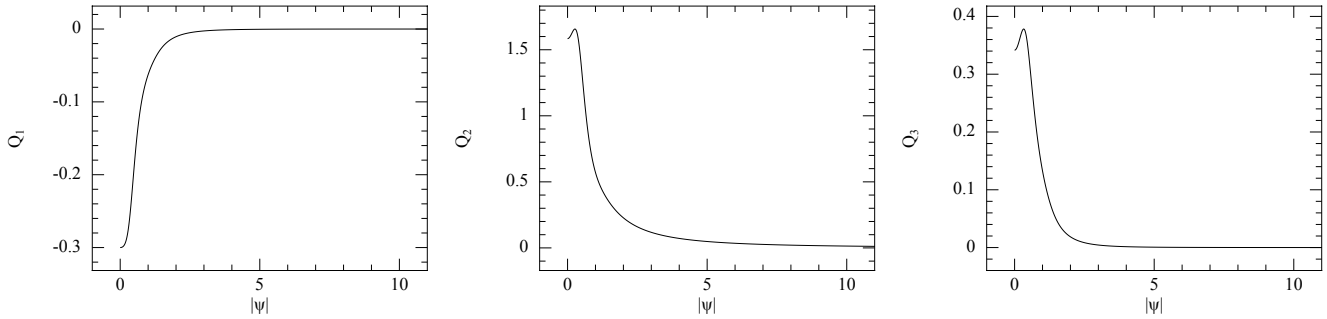

Figure 1. The effective viscosity coefficients Q_1, Q_2 and Q_3 plotted against warp amplitude $|\psi|$, assuming that $\alpha = 0.2$, $\alpha_b = 0$ and $\Gamma = 1$. The coefficients change significantly for $0 < |\psi| \lesssim 5$, after which they are approximately constant at a small but non-zero value

netic interaction of the disc with the spinning hole. This induces precessions in the disc orbits, and hence causes the angular momentum vector for each ring to precess around the spin vector for the black hole with a frequency

$$\mathbf{\Omega}_{\rm p} = \frac{2G\boldsymbol{J}_h}{c^2R^3} \tag{4}$$

with c the speed of light and G the gravitational constant. The magnitude of $\boldsymbol{J}_{\rm h}$ is given by $J_{\rm h} = acM(GM/c^2)$ where a is the dimensionless spin parameter and M is the mass of the hole (Kumar & Pringle, 1985). We include the back–reaction on the hole angular momentum vector $\boldsymbol{J}_{\rm h}$ by summing the effect of the precessions over all radii, giving the torque on the hole as:

$$\frac{{\rm d}\boldsymbol{J}_{\rm h}}{{\rm d}t} = -2\pi \int \mathbf{\Omega}_{\rm p} \times \boldsymbol{L}R{\rm d}R. \tag{5}$$

Since $\mathbf{\Omega}_{\rm p} \propto \boldsymbol{J}_{\rm h}$ this equation makes it clear that the magnitude of $\boldsymbol{J}_{\rm h}$ is conserved and hence $\boldsymbol{J}_{\rm h}$ can only precess on a sphere, simply because the LT torque has no component in the direction of $\boldsymbol{J}_{\rm h}$ for any disc structure. Equivalently the LT torque induces only precessions in the disc, so that the reaction back on the hole is simply a sum of precessions, which is itself a precession.

We integrate both (3) and (5) using a simple forward Euler method (Pringle, 1992) on a logarithmically spaced grid. However we adopt a different implementation of the boundary conditions. Rather than implementing a sink over a few grid cells we simply remove all of the angular momentum that reaches the inner– and outer–most cells at the end of each integration step. This allows angular momentum (and hence mass) to flow freely across the boundary, giving the usual $\Sigma = 0$, torque–free, accreting boundary condition. This is the form adopted in Lodato & Price (2010). We note that this boundary condition does not conserve angular momentum exactly. However this small effect does not affect the inclination of any of the rings and hence does not alter our results while the warp is propagating through the computational domain. Once the warp reaches the outer boundary it flows freely off the computational domain and the disc is flattened (i.e. we do not impose a boundary condition at the outer edge of the disc to maintain the disc warp).

2.2 Generating the constrained effective viscosities

We use the effective viscosities derived by Ogilvie (1999) for a locally isothermal disc. These are constrained to be consistent with the internal fluid dynamics of the disc, assuming an isotropic physical viscosity. The physics of these constraints is simply local conservation of mass and angular momentum in the disc.

The effective viscosities which describe the transport of angular momentum in a warped disc take the usual form of a Shakura & Sunyaev disc viscosity. The constraints determine the nonlinear coefficients (Q_1, Q_2, Q_3) of the effective viscosities (cf equations 10, 11 and 12). These coefficients all decrease in magnitude in the presence of a strong warp, where the disc rings are highly inclined to each other. Communication of angular momentum is reduced because the rings of gas are no longer in perfect contact. We expect angular momentum to be communicated through perturbations of the particles from circular orbits. The rate of communication, and hence the magnitude of the viscosities, therefore depend on how easily these particles can interact. This is harder for particles on inclined orbits, and once these reach a critical inclination this can only happen where the rings cross. We note that for inviscid discs, which we do not consider here, this interpretation is no longer valid, see Ogilvie (1999) for further details.

We now detail the calculation of the effective viscosities from the disc properties. The notation in Ogilvie (1999) differs from that in Pringle (1992). Our equation 3, and equation 122 from Ogilvie (1999) relate the effective viscosities (ν_1, ν_2 and ν_3) to the nonlinear viscosity coefficients (Q_1, Q_2 and Q_3) by

$$\nu_1 = \frac{Q_1 \mathscr{I}\Omega^2}{\Sigma R\frac{{\rm d}\Omega}{{\rm d}R}}, \tag{6}$$

$$\nu_2 = \frac{2Q_2 \mathscr{I}\Omega}{\Sigma} \tag{7}$$

and

$$\nu_3 = \frac{Q_3 \mathscr{I}\Omega}{\Sigma}, \tag{8}$$

where $\mathscr{I}$ is given by

$$\mathscr{I} = \frac{1}{2\pi}\int_0^{2\pi} \tilde{\mathscr{I}}\ {\rm d}\phi = \frac{1}{2\pi}\int_0^{2\pi}\int_{-\infty}^{\infty} \rho z^2\ {\rm d}z\ {\rm d}\phi. \tag{9}$$

Assuming Σ constant in azimuth, and a locally isothermal disc with sound speed c_s, we can write this as $\mathscr{I} \propto \Sigma c_s^2/\Omega^2$. For a point–mass potential with $\Omega = (GM/R^3)^{1/2}$ we get after some algebra

$$\nu_1 = -\frac{2}{3}Q_1\left[(H/R)^2\, R^2\Omega\right], \tag{10}$$

$$\nu_2 = 2Q_2\left[(H/R)^2\, R^2\Omega\right] \tag{11}$$

and

$$\nu_3 = Q_3\left[(H/R)^2\, R^2\Omega\right], \tag{12}$$

where $H = c_s/\Omega$ is the disc thickness.

For simplicity we assume that

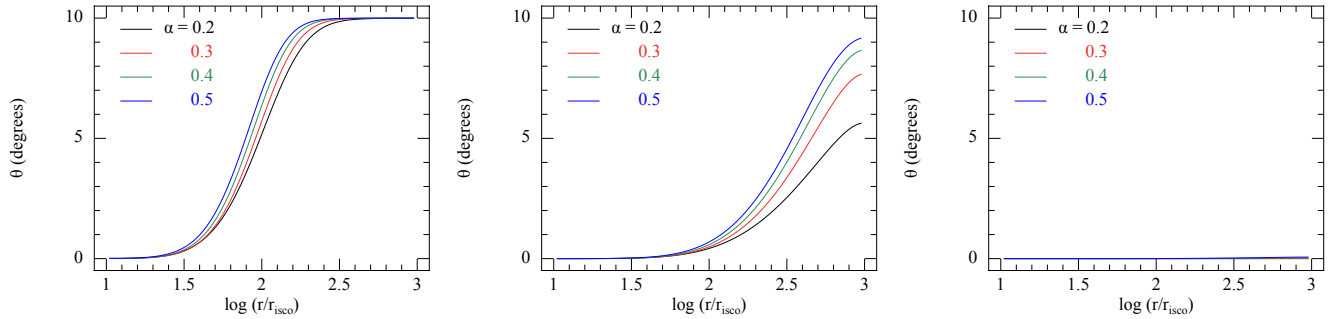

Figure 2. Disc structures for the constant effective viscosity simulations, given by plotting the tilt angle (θ) between the disc and the hole against the log of the radius. The initial misalignment of the disc is $\theta_0 = 10°$. On each plot the legend gives the value of α used in the simulation. From left to right the panels correspond to $t = 0.01$, 0.1 and 1 viscous times after the start of the calculation. Note that in the latter case the warp has moved to the edge of our grid and the disc aligns.

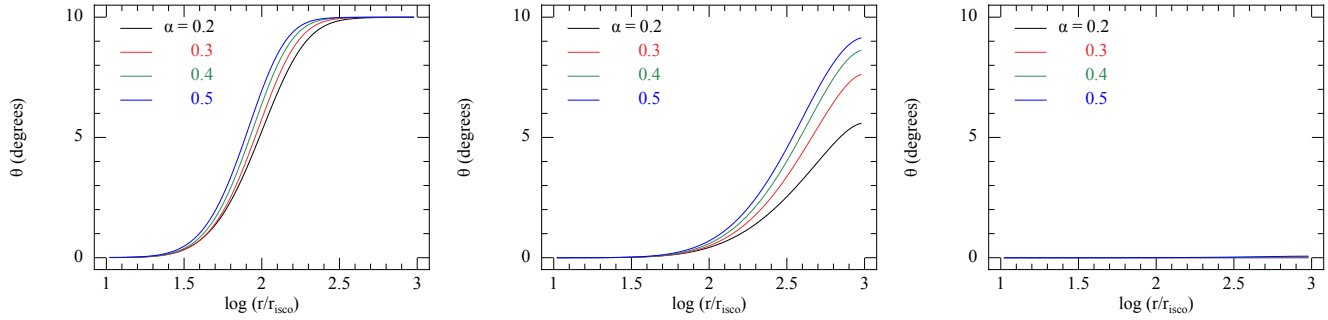

Figure 3. Disc structures for the full effective viscosity simulations, given by plotting the tilt angle between the disc and the hole against the log of the radius. The initial misalignment of the disc is $\theta_0 = 10°$. On each plot the legend gives the value of α used in the simulation. From left to right the panels correspond to $t = 0.01$, 0.1 and 1 viscous times after the start of the calculation. When compared to Fig. 2 this figure shows the negligible effect of the full effective viscosities when the misalignment between the disc and hole is small.

$$(H/R)^2 R^2 \Omega = \text{const.} \tag{13}$$

This removes the radial dependence of the viscosities, making them functions only of $|\psi|$ and α and so allowing a direct comparison with the constant viscosity simulations of Lodato & Pringle (2006). The assumption (13) requires that the sound speed $c_s \propto R^{-3/4}$. This compares with the usual steady–state disc, where $c_s \propto R^{-3/8}$ (e.g. Frank et al. 2002).

We note that for a disc without a warp, ν_1 reduces to exactly the usual α disc viscosity (Shakura & Sunyaev, 1973), since

$$\nu_1 = \alpha c_s H = \alpha (H/R)^2 R^2 \Omega \tag{14}$$

and

$$Q_1(|\psi| = 0) = -3\alpha/2. \tag{15}$$

The effective viscosities are now fixed by the nonlinear coefficients $Q_1(\alpha, |\psi|)$, $Q_2(\alpha, |\psi|)$ and $Q_3(\alpha, |\psi|)$. We calculate these coefficients in the same way as described in Ogilvie (1999) with $\Gamma = 1$ and $\alpha_b = 0$ using the code kindly provided by Gordon Ogilvie. Figure 1 show the coefficients plotted against the warp amplitude for $\alpha = 0.2$.

3 SIMULATIONS

We use the method described above to simulate the warping of a misaligned accretion disc under the LT effect. We set up our initially planar but misaligned disc on a logarithmically spaced grid from $R_{in} = 10R_{isco}$ to $R_{out} = 1000R_{isco}$ using 100 grid cells (where $R_{isco} = 6GM/c^2$ is the radius of the innermost stable circular orbit around a Schwarzchild black hole). The disc surface density is initially a Gaussian ring peaked at $R_0 = 500R_{isco}$ with width $50R_{isco}$. We initialise each ring with a constant misalignment angle, θ_0, such that the initial disc is flat but tilted to the plane of the black hole.

Lodato & Pringle (2006) suggest that the only governing parameters for simulations of this type are the ratio of disc to hole angular momenta (J_d/J_h), the ratio of the warp radius $R_w = \Omega_p R^3/\nu_2$ to R_0, and the ratio of the effective viscosities ν_2/ν_1 (note that they neglect ν_3). However, as we use the constrained effective viscosities, ν_2/ν_1 is now determined once we have chosen α.

The parameters that we are free to choose in these simulations are α, H/R, R_0, θ_0 and J_d/J_h. For black hole accretion discs $H/R \sim 10^{-3}$ and so we assume this throughout. Lodato & Pringle (2006) explored the effect of changing R_w/R_0, so we fix R_0 as above (note that this does not fix the ratio R_w/R_0. However this ratio varies little throughout our simulations.) To examine disc breaking we choose $J_d/J_h \ll 1$ as the simplest case and then vary α and θ_0.

3.1 Does the disc break?

We perform several simulations for $0.2 \leq \alpha \leq 0.5$ to determine the various nonlinear responses of the disc to warping. We do not simulate $\alpha < 0.2$ as this is where the viscosity ν_1 is predicted to become negative in strong warps. We simulate a range of θ_0 from 10°

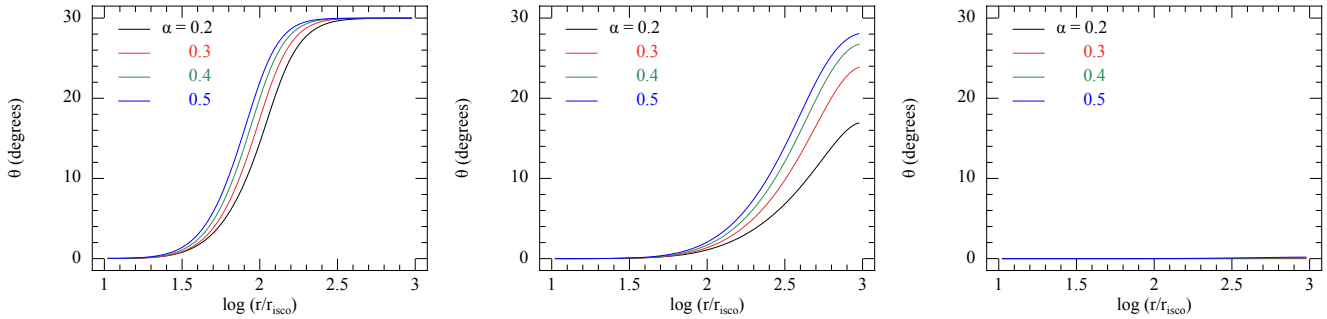

Figure 4. Disc structures for the constant effective viscosity simulations as in Fig. 2, but this time for initial misalignment $\theta = 30°$. From left to right the panels correspond to $t = 0.01$, 0.1 and 1 viscous times after the start of the calculation.

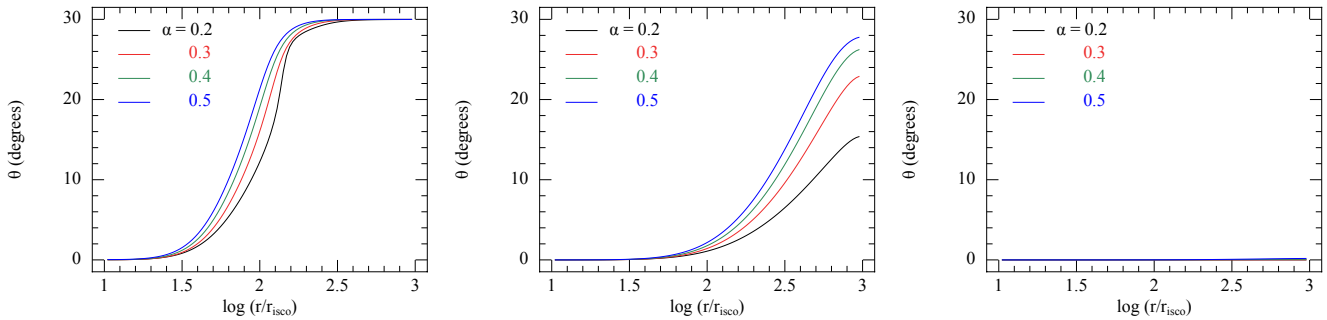

Figure 5. Disc structures for the full effective viscosity simulations as in Fig. 3, but this time for initial misalignment $\theta = 30°$. From left to right the panels correspond to $t = 0.01$, 0.1 and 1 viscous times after the start of the calculation. When compared to Fig. 4 this figure shows that even for a 30° misalignment angle the effect of the full effective viscosities can be small, however there is a steepening of the disc profile at early times for the $\alpha = 0.2$ simulations. This suggests that for the nonlinear effects to be important at $\theta_0 = 30°$ we need $\alpha \ll 0.2$.

to 60°. This allows us to explore the two regimes: $|\psi| \lesssim \alpha$, where nonlinear effects should be negligible, and $|\psi| \gtrsim \alpha$, where nonlinear effects should be important. Our setup corresponds to $J_d/J_h \approx 0.02$, with R_w/R_0 varying between ~ 0.95 and ~ 1.20 as α changes. Note that we evaluate (13) at R_0 with $H/R = 10^{-3}$.

We perform these simulations for two cases. In the first we use constant effective viscosities. This acts as a control so we can isolate the effect of introducing nonlinear dynamics in the second set of simulations, where we use the full effective viscosities. The constant effective viscosities are simply calculated using the method described in Section 2.2 with $|\psi| = 0$.

For the simulations involving constant effective viscosities we expect to recover the Bardeen–Petterson effect as seen by several other authors (e.g. Bardeen & Petterson 1975; Pringle 1992; Scheuer & Feiler 1996; Lodato & Pringle 2006 etc). However the simulations involving the full nonlinear effective viscosities should modify this somewhat.

3.1.1 $\theta = 10°$

In Fig. 2 we show the disc structures for simulations with $\theta_0 = 10°$ and the constant effective viscosities at 0.01, 0.1 and 1 t_{visc}. Here we define the viscous timescale as $t_{visc} = R_0^2/\nu_1$ with ν_1 evaluated for $|\psi| = 0$ and α as defined in the particular case. Fig. 2 shows the behaviour for different values of the disc viscosity parameter α. In this case the behaviour is similar for all simulations, with lower α aligning in a shorter fraction of the viscous time (although in reality more slowly because the viscous timescale is longer).

In Fig. 3 we show the same simulations as in Fig. 2. However this time we use the full effective viscosities. We expect the evolution here to be similar, as the warp is never able to achieve a large amplitude, making the viscosities similar in both cases. This is indeed the case, as there is no visible difference between Figures 2 & 3.

3.1.2 $\theta = 30°$

In Figures 4 & 5 we show the disc structures for simulations with $\theta_0 = 30°$. Again there is very little difference between the disc structures obtained using the constant effective viscosities and those with the full effective viscosities. However the disc profile steepens in the early stages of the $\alpha = 0.2$ simulation. This suggests that for $\theta = 30°$ we would have to go to $\alpha \ll 0.2$ to get disc breaking.

3.1.3 $\theta = 45°$

In Figures 6 & 7 we show the disc structures for simulations with $\theta_0 = 45°$. There is now a noticeable difference between the constant effective viscosity and full effective viscosity simulations. Even for large α the disc profile is steepened and for $\alpha \sim 0.2$ the disc breaks into two distinct planes. This break persists for more than a tenth of the viscous timescale for the disc. The disc aligns when the break propagates out to the edge of our grid which occurs at $t = 0.13 t_{visc}$.

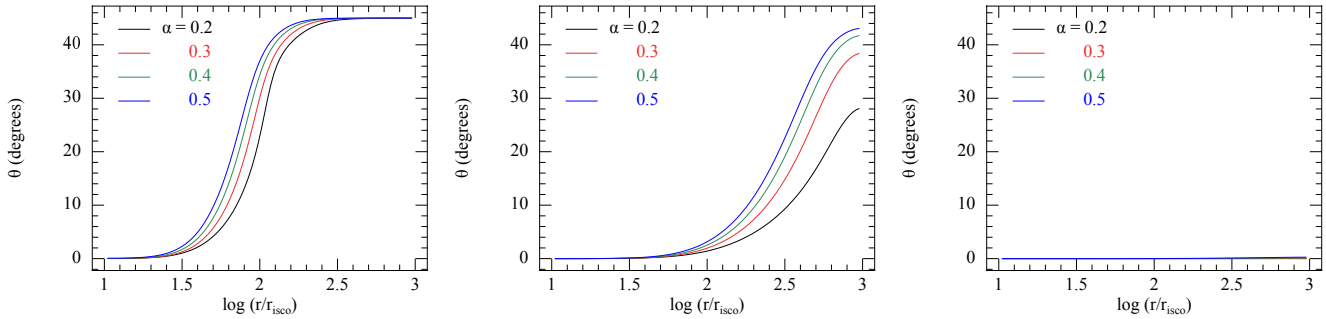

Figure 6. Disc structures for the constant effective viscosity simulations as in Fig. 2, but this time for initial misalignment $\theta = 45°$. From left to right the panels correspond to $t = 0.01$, 0.1 and 1 viscous times after the start of the calculation.

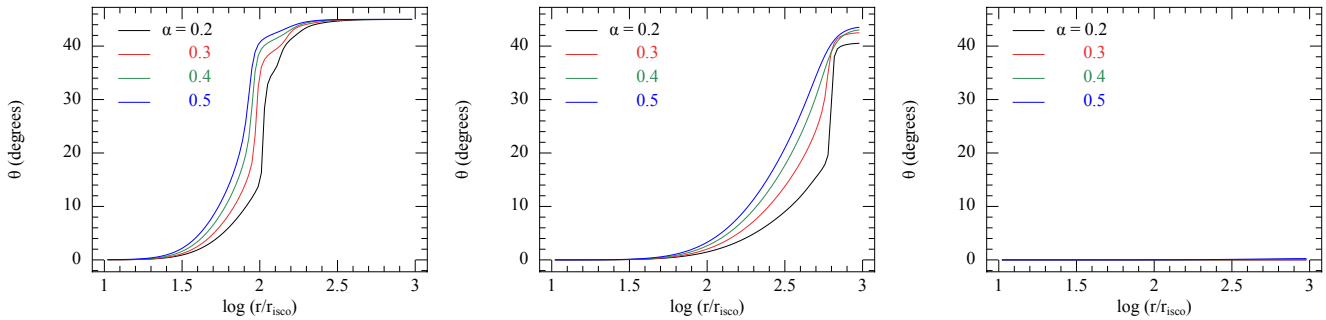

Figure 7. Disc structures for the full effective viscosity simulations as in Fig. 3, but this time for initial misalignment $\theta = 45°$. From left to right the panels correspond to $t = 0.01$, 0.1 and 1 viscous times after the start of the calculation. When compared to Fig. 6 this figure shows that the nonlinear effects can significantly influence the evolution of the disc. Here the profile is noticeably steepened at $t = 0.01t_{\rm visc}$ for all α. By $t = 0.1t_{\rm visc}$ the disc break is only maintained for small α. For $\alpha = 0.2$ the break propagates outwards in the disc until reaching the outer edge of the grid (at $t = 0.13t_{\rm visc}$) at which point the disc aligns. For larger α the disc is smoothed before it aligns.

3.1.4 $\theta = 60°$

In Figures 8 & 9 we show the disc structures for simulations with $\theta_0 = 60°$. There is again a noticeable difference between the constant effective viscosity and full effective viscosity simulations. At $t = 0.01t_{\rm visc}$ the disc profile is steepened noticeably more than in the $\theta = 45°$ case and by $t = 0.1t_{\rm visc}$ all of the simulations have maintained a break. We can also see that at $t = 0.01t_{\rm visc}$ in the constant effective viscosity simulation with $\alpha = 0.2$ it is possible for the disc to break without the nonlinear effects.

These simulations suggests two main results of using the full effective viscosities. First, discs can break for higher values of α, and second, discs can break for lower inclination angles.

There are two features of the simulations which we have not discussed so far. The first is the wiggles in the disc at the top of the warp in Figures 7 & 9. In these simulations the disc appears to try to break into more than just two distinct planes. It may be that for smaller α or larger $|\psi|$ the disc can break into more than two planes. However we deem this beyond the scope of the present investigation.

Second, the torques on the disc in the strong warp regions generate rapid mass flow rates into the ring inside the warp. This results in prominent spikes in $\Sigma(R)$ inside regions with large $|\psi|$. Increasing resolution only resolves these spikes better. We therefore leave the investigation of this effect to future work, which will require a different numerical method.

4 DISCUSSION

We have simulated the evolution of a misaligned accretion event on to a spinning black hole. Many previous simulations of this type assumed that the effective viscosities governing the angular momentum transport were constant. Here we have used effective viscosities constrained to be consistent with the internal fluid dynamics of the disc. We compare these results with those of equivalent simulations which assume constant effective viscosities. In the latter case we find that for small enough α the precession induced by the LT effect can cause the disc to break into two distinct planes if the misalignment is large enough. We also find that if we allow nonlinear effects (Ogilvie, 1999) the disc can break for higher values of α and smaller inclination angles. This suggests that nonlinear effects significantly change the evolution of strongly warped discs. The main effect is in reducing the magnitude of the effective viscosities in the warped region, noticeably reducing ν_1 more than ν_2. This reduces the disc's ability to smooth out the warp induced by the LT torque and so prevent a break. This is essentially a modified form of the Bardeen–Petterson effect, where the warp is steepened by the weakened disc response.

For small values of α, $\nu_2 \gg \nu_1$. Then the effective viscosity that tries to flatten tilted rings of gas is much stronger than the effective viscosity responsible for transporting angular momentum radially. However the ν_1 and ν_2 torques responsible for communicating angular momentum are proportional to $\boldsymbol{\ell}$ and $\partial\boldsymbol{\ell}/\partial R$ respectively. So to break the disc we also need a large warp. As $|\psi|$ increases the ν_2 torque becomes comparatively stronger that the ν_1 torque. When

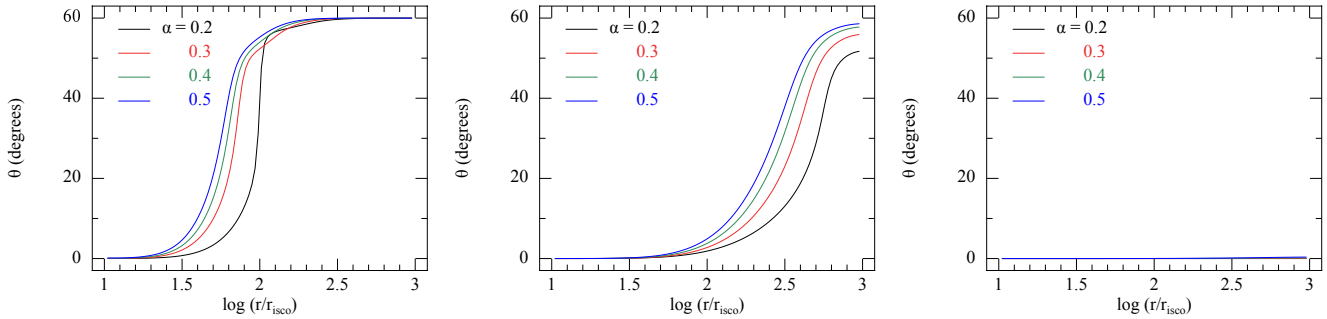

Figure 8. Disc structures for the constant effective viscosity simulations as in Fig. 2, but this time for initial misalignment $\theta = 60°$. From left to right the panels correspond to $t = 0.01$, 0.1 and 1 viscous times after the start of the calculation.

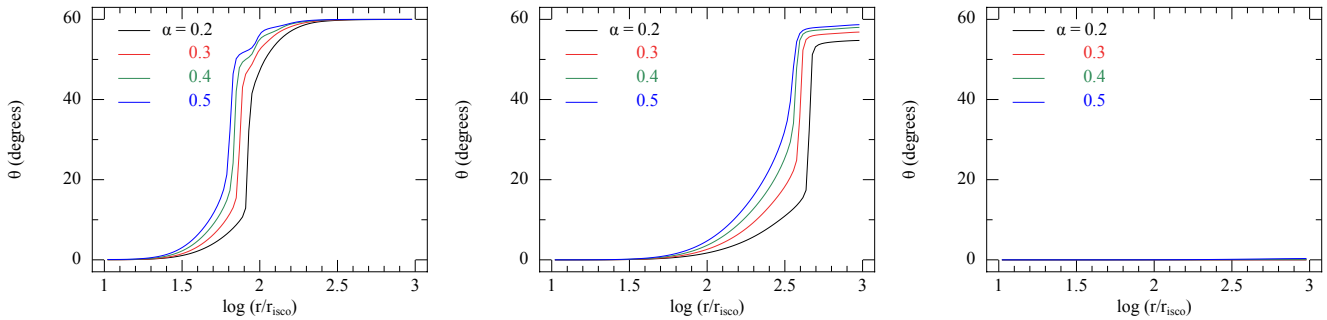

Figure 9. Disc structures for the full effective viscosity simulations as in Fig. 3, but this time for initial misalignment $\theta = 60°$. From left to right the panels correspond to $t = 0.01$, 0.1 and 1 viscous times after the start of the calculation. When compared to Fig. 8 this figure shows that the nonlinear effects can significantly influence the evolution of the disc. Initially the disc profile is significantly steepened for all α and the disc breaks for all α. This break propagates outwards in the disc until reaching the outer edge of the grid at which point the disc aligns.

the discrepancy between the magnitudes of the two torques is large enough the disc is effectively unable to communicate radially. As the differential precession induced by the LT effect acts faster at smaller radii, this allows the vertical effective viscosity (ν_2) to flatten each ring in turn into the plane of the spinning black hole. To maintain a smooth (small amplitude) warp the disc must be able to communicate radially on a timescale comparable to the flattening of rings into the plane of the black hole. When this does not hold the disc breaks.

For $\alpha \sim 1$ the disc can efficiently maintain a smooth warp. However for $\alpha \sim 0.2 - 0.4$ and a large misalignment we show there is a strong tendency for the disc to break under an external torque such as the LT torque. We see no reason for this behaviour to change when $\alpha \leq 0.1$. However there may be other nonlinear effects which become important here. The next step is a full 3D hydrodynamical numerical investigation to determine the disc response in this regime (e.g. Nelson & Papaloizou 2000; Lodato & Price 2010).

When the disc breaks it splits into a co– or counter–aligned inner disc and a misaligned outer disc. This break can propagate outwards and (dependent on α and θ_0) may persist until it reaches the outer regions of the disc. At this point the whole disc is co– or counter–aligned with the hole spin. This suggests that a break in the disc can be a long–lived feature, lasting for roughly the alignment timescale. We note that although we have not included any simulations of counter–aligning discs, it is already known that for $J_d/J_h \ll 1$ there is a symmetry in the behaviour of discs of this type around $\theta = 90°$ (King et al. 2005 and Lodato & Pringle 2006). Therefore the same behaviour would be seen in discs that are counter–aligning with the black hole (i.e. a misalignment of 120° would produce the same dynamics with a counter–aligning disc as the 60° case produces here).

For observational purposes it is important to compare the alignment timescale t_{al} with the lifetime t_{life} of the system. If $t_{al} > t_{life}$, the centre of the disc is never aligned with its warped outer plane. In an accreting stellar–mass black–hole binary this would mean that jets (which propagate along the axis of the central parts of the disc, and so the spin of the black hole) are in general misaligned with respect to the orbital plane. This is seen in the black–hole binary GRO J1655-40 (Martin et al. 2008 and references therein). Similarly the continuum–fitting method for estimating black–hole spins (Kulkarni et al. 2011 and references therein) uses the assumption that the black hole spin is aligned with the orbital axis in estimating the radiating disc area and hence the ISCO radius. It therefore implicitly requires $t_{al} < t_{life}$. In our simulations it is clear that discs are able to remain warped or broken for significant fractions of their viscous timescale. However we note that for strong warps there may be other nonlinear effects not included in the analysis of Ogilvie (1999) or additional dissipation caused by fluid instabilities (cf Gammie, Goodman & Ogilvie 2000). These may impact upon the alignment timescale.

It is also possible that the disc is never able to align fully; for example an accretion disc in a misaligned black hole binary system may be twisted one way by the LT effect and a different way by the binary torque (e.g. Martin et al., 2009). We therefore suggest careful consideration before assuming that black hole accretion discs

are aligned – particularly as Lodato & Pringle (2006) suggest that the accretion rate through warped discs is significantly enhanced, which suggests the possibility that strongly accreting discs are also strongly warped.

Disc breaking can have some important observational consequences. For example accretion discs in binary systems often have an outer disc aligned to the binary plane. However the inner disc (and so the direction of any jets) must be aligned with the black hole spin, which may be significantly misaligned with respect to the binary axis. Similarly breaks in protoplanetary discs may occur through the internal disc response to warping during formation of the disc, rather than being driven by the presence of a planet.

In this paper we have used a 1D Eulerian ring code to calculate the evolution of misaligned accretion events on to a spinning black hole. We caution that there is still much work to do before we can fully understand the evolution of such a disc. For example our treatment requires gas to orbit on circular rings, inherently excluding any effects which might break the cylindrical symmetry in the local disc plane. We also assume that the disc responds viscously, with no wave–like behaviour. The method also prevents us from examining exactly what happens in the disc break: by its nature, it occurs over only over a small number of rings and is therefore poorly resolved – however this does not affect our conclusion that the disc can break. The most frustrating restriction is the difficulty in simulating small enough α: the simulations we present here suggest that for small α nonlinear fluid effects can be particularly important. We will address these restrictions in future investigations.

We remark finally that although we have considered alignment effects induced by the LT effect on an accretion disc around a spinning black hole, the torque between a misaligned binary and an external accretion disc has a very similar form (Nixon, King & Pringle, 2011). Thus we expect similar phenomena to appear in that case. The enhanced accretion rates through the disc due to the dissipation in the warp (Lodato & Pringle, 2006) would increase the mass flow rate on to the binary. Therefore the coalescence timescale for the binary would be reduced further (Nixon et al., 2011).

ACKNOWLEDGMENTS

We thank the anonymous referee for valuable comments which helped to improve the manuscript. We thank Gordon Ogilvie for providing us with the routine to calculate the nonlinear viscosity coefficients. We also thank Jim Pringle, Gordon Ogilvie, Richard Alexander and Giuseppe Lodato for useful discussions. CJN holds an STFC postgraduate studentship. We acknowledge the use of SPLASH (Price, 2007) for generating the figures. Research in theoretical astrophysics at Leicester is supported by an STFC Rolling Grant. This research used the ALICE High Performance Computing Facility at the University of Leicester. Some resources on ALICE form part of the DiRAC Facility jointly funded by STFC and the Large Facilities Capital Fund of BIS.

REFERENCES

Arzoumanian Z., Chernoff D. F., Cordes J. M., 2002, ApJ, 568, 289
Bardeen J. M., Petterson J. A., 1975, ApJ, 195, L65+
Frank J., King A., Raine D. J., 2002, Accretion Power in Astrophysics: Third Edition
Gammie C. F., Goodman J., Ogilvie G. I., 2000, MNRAS, 318, 1005
Hobbs G., Lorimer D. R., Lyne A. G., Kramer M., 2005, MNRAS, 360, 974
King A. R., Lubow S. H., Ogilvie G. I., Pringle J. E., 2005, MNRAS, 363, 49
King A. R., Pringle J. E., 2006, MNRAS, 373, L90
King A. R., Pringle J. E., 2007, MNRAS, 377, L25
King A. R., Pringle J. E., Hofmann J. A., 2008, MNRAS, 385, 1621
Kulkarni A. K., Penna R. F., Shcherbakov R. V., Steiner J. F., Narayan R., Sä Dowski A., Zhu Y., McClintock J. E., Davis S. W., McKinney J. C., 2011, MNRAS, 414, 1183
Kumar S., Pringle J. E., 1985, MNRAS, 213, 435
Larwood J. D., Papaloizou J. C. B., 1997, MNRAS, 285, 288
Lense J., Thirring H., 1918, Phys. Z., 19, 156
Lodato G., Price D. J., 2010, MNRAS, 405, 1212
Lodato G., Pringle J. E., 2006, MNRAS, 368, 1196
Martin R. G., Pringle J. E., Tout C. A., 2009, MNRAS, 400, 383
Martin R. G., Tout C. A., Pringle J. E., 2008, MNRAS, 387, 188
Nelson R. P., Papaloizou J. C. B., 2000, MNRAS, 315, 570
Nixon C. J., Cossins P. J., King A. R., Pringle J. E., 2011, MNRAS, 412, 1591
Nixon C. J., King A. R., Pringle J. E., 2011, MNRAS, pp L311+
Ogilvie G. I., 1999, MNRAS, 304, 557
Papaloizou J. C. B., Pringle J. E., 1983, MNRAS, 202, 1181
Price D. J., 2007, Publ. Astron. Soc. Aust., 24, 159
Pringle J. E., 1992, MNRAS, 258, 811
Scheuer P. A. G., Feiler R., 1996, MNRAS, 282, 291
Shakura N. I., Sunyaev R. A., 1973, A&A, 24, 337
Shklovskii I. S., 1970, Soviet Ast., 13, 562
Sutantyo W., 1978, Ap&SS, 54, 479